On the other hand, introduction of vibrations can stabilize all modes simultaneously, as it was in the case of glow discharge.

2) The main results of this paper were presented at several seminars and in the course of all of them the question was asked: Is it possible to stabilize the system using not regular but random "vibrations"? Since I strongly suspect that the same question may also appear now, I would like to give some comments.

The answer to the stated question is not found, although it was discussed in many publications (see, for instance, [14], [15]), and some particular result concerning first- and second-order systems were obtained. In the light of the present study, a plausible conjecture can be posed.

Hypothesis: Let system $\dot{x}=Ax$ be observable *in principle*. Then the condition tr $A<0$ is necessary and sufficient for the existence of the stationary ergodic matrix random process $W(t)=\|w_{ij}(t)\|_{i,j=1}^{n}$ (with zero mean) such that system $\dot{x}=(A+W(t))x$ is asymptotically stable with a probability of one.

Acknowledgment

The author would like to express his gratitude to three anonymous reviewers for their constructive comments.

References

[1] N. N. Boboliubov, *On Some Statistical Methods in Mathematical Physics* (in Russian). Kiev, Ukr. Acad. Sci. Publishers, 1945.

[2] S. M. Meerkov, "Averaging of trajectories of slow dynamic systems," *Differential Equations*, vol. 9, pp. 1239–1245, 1973.

[3] ——, "Vibrational control theory," *J. Franklin Inst.*, pp. 117–128, 1977.

[4] M. S. Livingston, *High-Energy Accelerators*. New York: Wiley-Interscience, 1954.

[5] A. M. Soroka and G. I. Shapiro, "Ionisation thermal instability in the glow discharge plasma," *Phys. Plasma*, vol. 6, pp. 879–883, 1975.

[6] S. M. Meerkov and G. I. Shapiro, "Method of vibrational control in the problem of stabilization of ionization-thermal instability of a powerful continuous CO_2 laser," *Automat. Remote Contr.*, vol. 37, pp. 821–830, 1976.

[7] S. M. Osovets, "Dynamic methods of retention and stabilization of plasma," *Uspehi Fizicheskih Nauk*, vol. 112, pp. 637–684, 1974.

[8] B. P. Demidovich, *Lectures on Mathematical Theory of Stability* (in Russian). Moscow: Nauka, 1967, p. 167.

[9] R. Gabasov and F. Kirillova, *Qualitative Theory of Optimal Processes* (in Russian). Moscow: Nauka, 1971.

[10] D. Graupe, *Identification of Systems*. Huntington, NY: Krieger, 1976.

[11] S. M. Meerkov and M. Yu. Tsitkin, "The effectiveness of the method of vibrational control for the dynamic systems of the order n," *Automat. Remote Contr.*, vol. 36, pp. 525–529, 1975.

[12] S. M. Meerkov, "Vibrational control," *Automat. Remote Contr.*, vol. 34, pp. 201–209, 1973.

[13] I. A. Generalov, V. P. Zimakov, V. D. Kosinkin, Yu. P. Raizer, and D. I. Roitenburt, "A method for substantial increase of discharge stability in fast flux large volume laser," *Pis'ma v Zurnal Technicheskoi Fiziki*, vol. 1, 1975.

[14] M. A. Leibowits, "Statistical behavior of linear systems with randomly varying parameters," *J. Math. Phys.*, vol. 4, pp. 852–858, 1963.

[15] R. Z. Khasminsky, *Stability of Systems of Differential Equations with Random Disturbances of Their Parameters* (in Russian). Moscow: Nauka, 1969.

Statistical Analysis of a Two-Ellipsoid Overlap Test for Real-Time Failure Detection

THOMAS H. KERR, MEMBER, IEEE

***Abstract*—Real-time failure detection for systems having linear stochastic dynamical truth models has been posed in terms of two confidence region sheaths in [1]–[3]. One confidence region sheath is about the expected nominal no-failure trajectory; the other is about the Kalman estimate of the state(s) being monitored for failures. The implementation of a necessary and sufficient test of whether these two confidence regions of elliptical cross section are disjoint at any time instant is shown to result in a scalar test statistic that is compared to a prespecified decision threshold at each check-time in making failure/no-failure decisions.**

The motivating theoretical basis of the test statistic is briefly discussed, the implementation equations and theoretical milestones previously encountered in guaranteeing algorithm convergence and establishing convergence rate are summarized, then the details are presented for:

1) the derivation and analytic evaluation of the expressions for the probabilities of false alarm and correct detection that serve as a basis for subsequent tradeoffs in setting the threshold level; and

2) the derivation of an expression for the decision threshold and a technique for its calculation from the covariance of the Kalman filter.

The probability of correct detection is shown to be a monotonely increasing function of the underlying fundamental signal-to-noise ratio response of the Kalman filter estimate of the failure mode state to a particular magnitude of failure. Real data results are provided to illustrate application of this technique for the two-dimensional case to detect failures in an inertial navigation system having two-degree-of-freedom gyros. This is the application for which the technique was developed.

Manuscript received December 16, 1976; revised June 3, 1977 and December 14, 1979. Paper recommended by Y. Bar-Shalom, Past Chairman of the Stochastic Control Committee. This work was supported by the Department of the Navy, Strategic Systems Project Office, under Contract N00030-75-C-0081.

The author was with The Analytic Sciences Corporation, Reading, MA 01867. He is now with Intermetrics, Inc., Cambridge, MA 02138.

I. Introduction

Whereas the detection of an unknown signal at a known event time or the detection of a known signal at an unknown time are standard problems in communication theory as presented in [4]–[7], the problem in failure detection is to detect a signal of unknown magnitude which occurs at an unknown time. Failure detection in a dynamic stochastic system is a more difficult problem that has only relatively recently received attention in the literature [3], [8, References 5, 9, 12, 15, 16, 22, 24, 26, 28, 29, 31, 33, 52], as discussed in the failure detection survey, and in [9]–[20]. Each of the above cited references represents a different approach to failure detection.

Most of the above proposed failure detection methods utilize a statistical test which relies on the whiteness property of the Kalman filter innovations or residuals [24, pp. 597–606]. However, a reduced-state filter is required in many practical implementations to avoid an otherwise unacceptable computational burden or to avoid poor sensitivity characteristics [29, p. 279]. Filter residuals may be nonwhite either because of a failure occurring or because of the required use of a reduced-order or "densensitized" filter for practical reasons [29, pp. 230–232]. Therefore, when using a statistical test that only checks for white residuals a dilemma arises from the difficulty of distinguishing between the nonwhite residuals due to a nominal unfailed system that is implemented with a "practical" filter [21]–[23] and the nonwhite residuals that arise from an actual occurrence of failure.

The so-called two-confidence region failure detection approach has been developed [1]–[3] which is based on the multidimensional confidence regions associated with the underlying Gaussian random processes under both failure and no-failure. The Gaussian processes persist even if a suboptimal filter is used as long as the filter is linear. This failure detection approach also uses the estimates and covariances of error of a linear filter, *but does not depend on there being white innovations in the nominal unfailed situation* (further details on the use of a suboptimal filter are found at the end of Section VII).

The contribution of this paper is in the derivation of the general expressions for the off-line statistical analysis of the two-confidence region decision test in terms of the probabilities of false alarm P_{fa} and correct detection P_d. A technique is specified for numerical quantification of P_{fa} and P_d for the scalar and two-dimensional cases and the technique is used in an inertial navigation system application.

To date, a detailed statistical analysis in support of a failure detection technique that has been proposed for specific navigation applications is available in the open literature as [20]. However, an assumption in [20] for the nominal unfailed operating condition, is that the gyro drifts of that application are negligible as compared to gimbal angle resolver quantization error so the test statistic for calculating P_{fa} is consequently taken to be a function of only the gimbal angle quantization error. In the real-time application of the two-confidence region failure detection approach to an inertial navigation system (INS) presented in Section III, the test statistic is specifically a function of the gyro drift-rate states that are modeled in the filter because an objective is to detect large anomalous excursions of the gyro drift-rate as a failure.

0018-9286/80/0800-0762$00.75 ©1980 IEEE

II. Motivation for Using Two Confidence Regions to Detect Failures

The two-confidence region approach to failure detection may be applied to systems that have either truth models or error models that may be represented in the following linear state variable form:

$$x(k+1)=\Phi(k+1,k)x(k)+w(k)+\nu\delta_{k,\theta} \tag{1}$$

$$z(k)=H(k)x(k)+v(k) \tag{2}$$

where $w(k)$ and $v(k)$ are independent, zero-mean, Gaussian white noises, having covariances of intensity $Q(k)$ and $R(k)$, respectively, and $x(0)$ is a Gaussian random vector initial condition (independent of the noises) of mean x_0 and variance P_0. The failure modes that can be monitored using this two-confidence region approach can be modeled as states of the system (1) (e.g., unwanted deleterious ramp and bias gyro drift-rates and accelerometer biases are examples of soft or subtle failures that may be modeled as states in the linear error model of an INS [9]). A failure may be represented[1] [8, eq. 40] as the vector ν (unknown magnitude and direction unknown but confined to the subspace spanned by the modeled failure mode states) that occurs at the unknown failure time θ. The event of a failure occurring is commonly represented by the Kronecker delta $\delta_{k,\theta}$, that is, unity for $k=\theta$ and zero otherwise.

Unlike the situations for which the usual likelihood ratio is a uniformly most powerful (UMP) test in that it is as good as or better than any other decision test [5, p. 91], [6, p. 102], the failure event to be detected is a random event that occurs at a random or unknown time. There is a little justification for using a likelihood ratio as a decision function [27, p. 315] since it is not UMP for this situation of unknown failure time and there may be other decision functions that are as good or better[2] [5, pp. 91–96]. Confidence region tests serve as an alternative approach although no formal proof is yet available to demonstrate that they are necessarily better or worse than a likelihood ratio approach. However, confidence region approaches have recently been proposed for other detection applications as well [28].

A Kalman filter, modeled on the unfailed system of (1) with the term $\nu\delta_{k,\theta}$ absent, is implemented to track the system that is to be monitored for failures. The Kalman filter uses the measurements $z(k)$ as inputs and the estimate $\hat{x}(k)$ evolves from an iteration equation which has the following form (by combining propagate and update stages [29]) as

$$\hat{x}(k+1)=\Phi(k+1,k)\hat{x}(k)+K(k+1)[z(k+1)-H\Phi(k+1,k)\hat{x}(k)] \tag{3}$$

$$\hat{x}(0)=x_0$$

with the covariance of error in estimation being provided from the following iteration equation:

$$P_1(k+1)=\Phi(k+1,k)[I-K(k)H(k)]P_1(k)\Phi^T(k+1,k)+Q(k+1) \tag{4}$$

$$P_1(0)=P_0$$

and with the Kalman gain, as used in (3), being defined as

$$K(k)=P_1(k)H^T(k)\left[H(k)P_1(k)H^T(k)+R(k)\right]^{-1}. \tag{5}$$

In order to use two confidence regions for failure detection, the expected value of the unfailed system and the associated variance available, without using the measurements, are needed and are provided, respectively, as solutions of the following two iteration equations:

$$\bar{x}(k+1)=E[x(k+1)|H_0]=\Phi(k+1,k)\bar{x}(k) \tag{6}$$

$$\bar{x}(0)=x_0$$

$$P_2(k+1)=\Phi(k+1,k)P_2(k)\Phi^T(k+1,k)+Q(k+1) \tag{7}$$

$$P_2(0)=P_0.$$

The underlying alternative hypothesis for the failure mode states x_i are

$$\text{(no-failure)} \quad H_0\colon \hat{x}_i(k)\sim N(0,[P_{\hat{x}\hat{x}}(k)]_{ii}) \quad \text{(zero mean)} \tag{8}$$

$$\text{(failure)} \quad H_1\colon \hat{x}_i(k)\sim N(d(k),[P_{\hat{x}\hat{x}}(k)]_{ii}) \quad \text{(nonzero mean)} \tag{9}$$

where $d(k)$ is defined as

$$d(k)\triangleq i\text{th component of the mean deterministic response of the filter to an assumed specific failure mode } \bar{\nu} \text{ that is to be detected}^3 \tag{10}$$

and

$$P_{\hat{x}_i\hat{x}_i}(k) \text{ is the } (i,i)\text{th component } [P_{\hat{x}\hat{x}}(k)]_{ii} \text{ of}$$

$$P_{\hat{x}\hat{x}}(k)=P_2(k)-P_1(k)>0 \qquad \text{for } k>0. \tag{11}$$

(Equation (11) follows from an application of the projection theorem [30, p. 202].)

Figure 1 presents the principle underlying the so-called two-confidence interval hypothesis test for distinguishing between H_0 and H_1 at time$=k$. The two confidence intervals that are being tested for overlap are depicted as lying along the horizontal axis. One confidence interval is centered about the expected unfailed value of zero and reflects the uncertainty of the system noise by the conservative extension to $\pm n(k)\cdot\sqrt{[P_2(k)]_{ii}}$. The other confidence region is centered about the Kalman estimate $\hat{x}_i(k)$, which itself reflects the current information obtained from the measurements[4], within the uncertainty of the system and measurement noise conservatively included in the extension of $\pm n(k)\cdot\sqrt{[P_2(k)]_{ii}}$. *As long as the two confidence intervals overlap, the true state $x_i(k)$ may be in both confidence intervals; however, when both confidence intervals are disjoint, the true state cannot be in both intervals simultaneously and a failure is declared.*

An obvious test for the overlap of the two confidence intervals is to compare the endpoints of the two intervals. From Fig. 1, it is seen that there is no overlap either if

$$n(k)\cdot\sqrt{[P_1(k)]_{ii}}+n(k)\cdot\sqrt{[P_2(k)]_{ii}}<\hat{x}_i(k) \tag{12}$$

or if

$$\hat{x}_i(k)<-n(k)\cdot\sqrt{[P_1(k)]_{ii}}-n(k)\cdot\sqrt{[P_2(k)]_{ii}}. \tag{13}$$

This decision rule may be concisely written by combining (12) and (13) as

NO OVERLAP (DECLARE FAILURE) WHEN:

$$|\hat{x}_i(k)|>n(k)\cdot\left(\sqrt{[P_2(k)]_{ii}}+\sqrt{[P_1(k)]_{ii}}\right) \tag{14a}$$

OVERLAP (NO-FAILURE) WHEN:

$$|\hat{x}_i(k)|\leq n(k)\cdot\left(\sqrt{[P_2(k)]_{ii}}+\sqrt{[P_1(k)]_{ii}}\right). \tag{14b}$$

An alternate test for the overlap of the two confidence intervals results from considering the associated parabolas[5] of Fig. 1. First, notice that the image in the range of each of the four endpoints of the two confidence intervals is $[n(k)]^2$. The decision threshold at time$=k$ is

$$K_1(k)\triangleq[n(k)]^2 \tag{15}$$

but specification of the exact value of $n(k)$ is deferred to Section VI.

[1]The two-confidence region approach can also be used to detect time-varying failures.

[2]The generalized likelihood ratio (GLR) has been described as an "optimum decision rule" for failure detection [8, p. 607], but no criterion was provided in support of this claim to indicate how it would be optimum. Indeed, four caveats have been cited [6, p. 106] for use of a likelihood ratio in conjunction with a maximum likelihood estimate as done with GLR.

[3]The time history of the parameter $d(k)$ may be evaluated through a simulation using the truth model with the system and measurement noise sample functions zeroed out and only the $\bar{\nu}$ failure mode activated.

[4]Matching the filter to the "no-failure" model may require "tuning" [29, p. 279] of the covariance $Q(k)$ so that the filter bandwidth remains open to prevent subsequent measurements from being ignored.

[5]These two parabolas correspond to the exponent of the Gaussian densities for $x_i(k)$ at time$=k$ from the Gauss–Markov system of (1) and as the solution of the Stratonovich–Kushner–Bucy equation [30, p. 178], respectively.

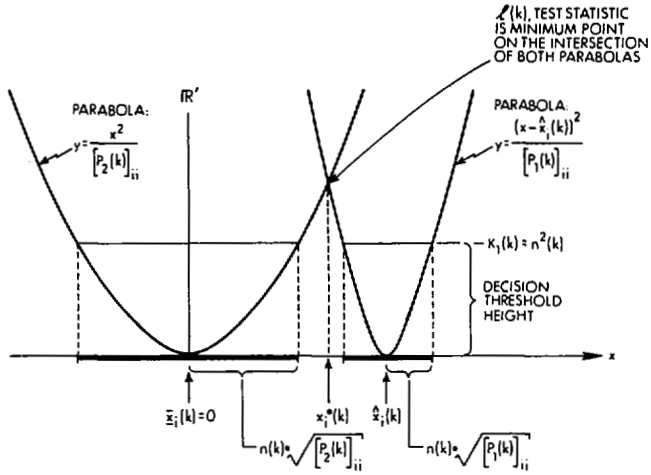

Fig. 1. Confidence intervals and associated parabolas at time $=k$ for two-confidence interval failure detection.

From Fig. 1, notice that $x_i^*(k)$ (i.e., the point in the domain that corresponds to the minimum point on the intersection of both parabolas) serves a special function. If the two intervals overlap, they both contain $x_i^*(k)$. If the two intervals are disjoint, neither contains $x_i^*(k)$. Consequently, *the presence of the special point $x_i^*(k)$ in either of the two confidence intervals is necessary and sufficient for overlap of the intervals.* This special point $x_i^*(k)$ may be conveniently found as the solution of the constrained nonlinear optimization problem having the following Lagrangian:

$$L(x_i,\lambda)=\left[(x_i-\hat{x}_i)^2/[P_1]_{ii}\right]+\lambda\left\{-\left[(x_i-\hat{x}_i)^2/[P_1]_{ii}\right]+\left[x_i^2/[P_2]_{ii}\right]\right\} \tag{16}$$

where λ is a scalar Lagrange multiplier and the term in braces represents the constraint that the minimum be on the intersection of the two parabolas. The optimization problem may be conveniently solved analytically for this case of one-dimensional confidence intervals by progressing as described below. Solve for the critical points of $L(x_i,\lambda)$ by the following.

1) Differentiating (16) with respect to x_i, setting the result to zero, and solving for x_i as shown in (17) and (18), respectively:

$$0=\frac{\partial L(x_i,\lambda)}{\partial x_i}=2(1-\lambda)[(x_i-\hat{x}_i)/[P_1]_{ii}]+2\lambda[x_i/[P_2]_{ii}] \tag{17}$$

$$x_i=(1-\lambda)[P_2]_{ii}\hat{x}_i/[(1-\lambda)[P_2]_{ii}+\lambda[P_1]_{ii}]. \tag{18}$$

2) Differentiating (16) with respect to λ, setting the result to zero, and substituting for x_i from (18) yields

$$[1-(\hat{x}_i^2[P_1]_{ii}/\hat{x}_i^2[P_2]_{ii})]\lambda^2-2\lambda+1=0 \tag{19}$$

a quadratic equation that λ^* must satisfy.[6]

3) Upon solving the quadratic equation of (19), choosing the correct sign to yield the minimum rather than the maximum, the correct Lagrange multiplier is

$$\lambda^*=\sqrt{[P_2]_{ii}}\,/\left(\sqrt{[P_2]_{ii}}+\sqrt{[P_1]_{ii}}\right). \tag{20}$$

4) Substituting the scalar λ^* from (20) back into (18) results in an expression for the special point as

$$x_i^*=\sqrt{[P_2]_{ii}}\,\hat{x}_i/\left(\sqrt{[P_2]_{ii}}+\sqrt{[P_1]_{ii}}\right). \tag{21}$$

5) Checking that x_i^* corresponds to the intersection of the two parabolas of Fig. 1, substitution of (21) into both parabola equations results in the anticipated equality as

$$L(x_i^*,\lambda^*)=y(x_i^*(k))=[\hat{x}_i(k)]^2/\left(\sqrt{[P_2(k)]_{ii}}+\sqrt{[P_1(k)]_{ii}}\right)^2 \tag{22}$$

6) Defining the test statistic at time $=k$ as

$$l(k)\triangleq L(x_i^*(k),\lambda^*(k))=[\hat{x}_i(k)]^2/\left(\sqrt{[P_2(k)]_{ii}}+\sqrt{[P_1(k)]_{ii}}\right)^2 \tag{23}$$

allows the alternate overlap/no-overlap decision test of Fig. 1 to be performed in the range using $l(k)$, rather than in the domain using $x_i^*(k)$. The equivalent[7] alternative decision rule in the range compares the test statistic $l(k)$ of (23) to the decision threshold $K_1(k)$ of (15) as

NO OVERLAP (DECLARE FAILURE) WHEN:

$$l(k)>K_1(k) \tag{24a}$$

OVERLAP (NO-FAILURE) WHEN:

$$l(k)\leqslant K_1(k). \tag{24b}$$

While the obvious decision rule of (14) was easy to obtain as a test for the overlap/nonoverlap of confidence intervals *it is the alternate formulation of the decision rule as* (24) *that generalizes to two or more dimensions.* (The use of one two-dimensional two-confidence region test is more appropriate than the use of two similar scalar tests in seeking to detect drift-rate failures in two-degree-of-freedom gyros that utilize two input axes. With a two-dimensional test, tilt or skewness information, intrinsically contained in the cross correlations, is not neglected as it would be if two scalar tests were used to monitor these axes. An additional advantage of using a two-dimensional confidence region test over using two scalar confidence interval tests for this application is the larger underlying signal-to-noise ratio (SNR) response to a failure, available for subsequent processing at the input of the failure detection algorithm, as demonstrated in Appendix A.)

A summarizing overview is provided in Fig. 2 of how this failure detection approach generalizes to the multidimensional case (treated in [3]). The top diagram depicts the two confidence regions of elliptical cross section which indicate a failure at the check times at which they fail to overlap. At each check time t_i, the elliptical cross sections of the top diagram are fixed levels of two paraboloids, shown in the middle diagram. This is where the overlap test is formulated as the solution of a minimization problem. A necessary and sufficient test for disjoint confidence region ellipses is that $l(t_i)$, the minimum point of the intersection of the two paraboloids, be above $K_1(t_i)$ (which can be determined by monitoring only the scalar test statistic history and decision threshold in the bottom diagram). A more detailed explanation of Fig. 2 can be found in [3, Section 6] where the six steps for mechanization are presented in a table to demonstrate how simple the CR2 test is to implement. Analytical expressions are derived in Sections VI and VII which are used to calculate the time-varying decision threshold K_1 and for evaluating the detection and false alarm probabilities associated with this decision test.

III. Summary of Previous Supporting Theoretical Derivations

As established in [3], the decision rule of (24) can be applied directly to the failure/no-failure decision test for two multidimensional confidence regions by using the following test statistic:

$$l(\lambda^*,k)=\lambda^*(1-\lambda^*)\hat{x}^T(k)[(1-\lambda^*)P_2(k)+\lambda^*P_1(k)]^{-1}\hat{x}(k) \tag{25}$$

where λ^* is the solution of the following scalar iteration equation:

$$\lambda_{n+1}=1/[1+(\hat{x}^T(k)A^{-1}(\lambda_n)P_1A^{-1}(\lambda_n)\hat{x}(k)/\hat{x}^T(k)A^{-1}(\lambda_n)\hat{x}(k))] \tag{26}$$

where

$$A(\lambda_n)\triangleq[(1-\lambda_n)P_2(k)+\lambda_nP_1(k)] \tag{27}$$

with λ_0 chosen (as explained in [3, Section 5]) so that

[6] In the multidimensional case, the $\hat{x}$'s occur in an inner product in (19) and do not divide out; the solution for λ in the multidimensional case requires an iterative equation. The derivation of (17)–(23) is supplied to enable a contrast between the simple scalar results presented here and the slightly more complex results of [3] for the general multidimensional case.

[7] That the decision rule of (24) is identical to that of (14) may be verified by using the definition of $l(k)$ and $K_1(k)$ from (23) and (15), multiplying through by the covariances and taking square roots throughout.

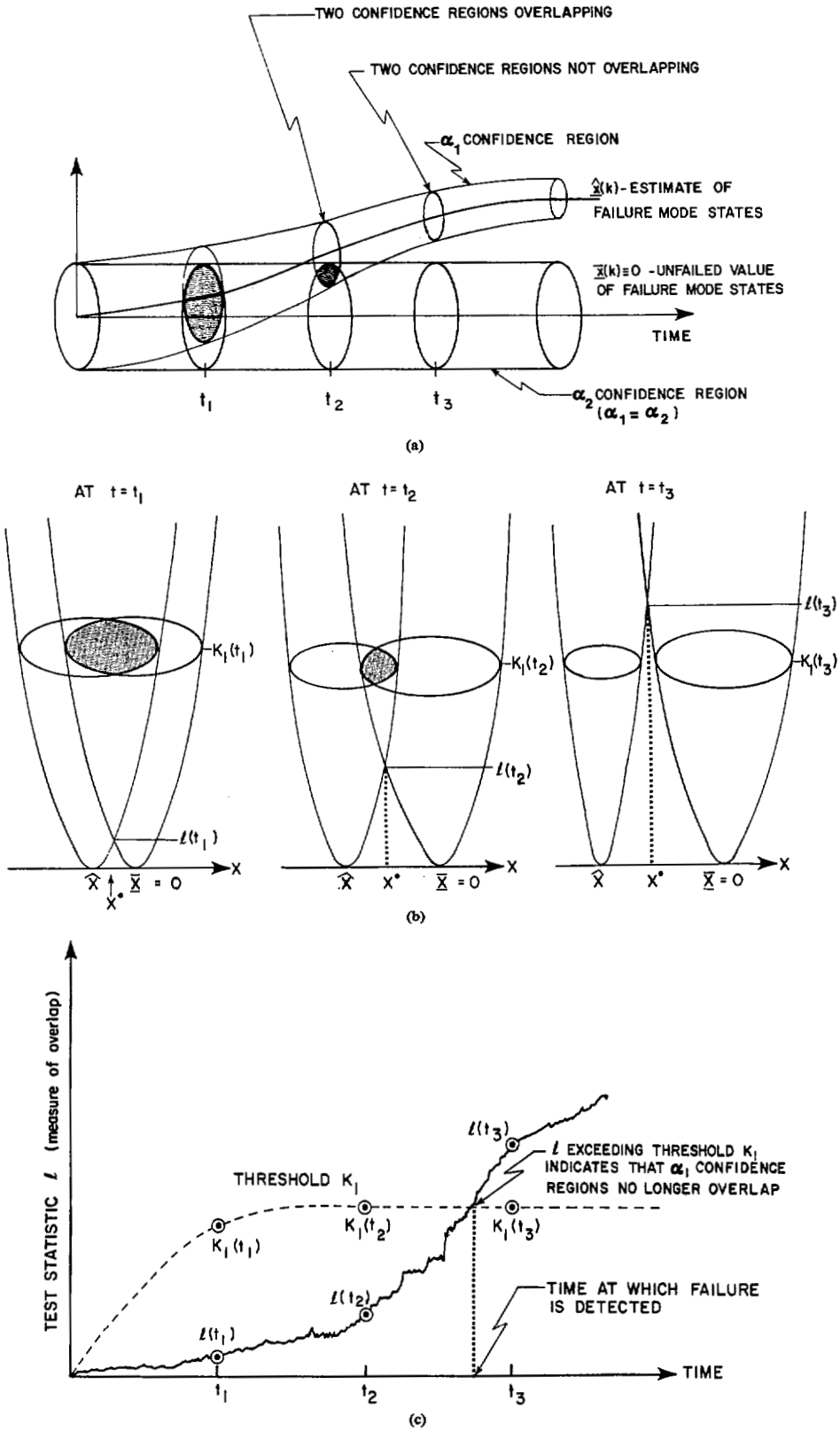

Fig. 2. Overview shows how comparison of scalar test statistic to decision threshold related to test for confidence region overlap through artifice of optimization problem. (a) Two confidence regions. (b) A new optimization at each time. (c) CR2 failure detection.

$$\frac{1}{2} < \lambda_0 < 1.$$

Subsequent to an early iterative technique proposed for calculating the test statistic in [1], [2], the better iterative algorithm of (26) and a stronger convergence proof based on the property of a contraction mapping [32] have been obtained as (34) and [3, Theorem 5.1], respectively. The convergence proof *guarantees* that, for the system of equations (1) and (2) which is "stabilizable and detectable,"[8] the *iterative algorithm will always converge*. By using another property of contraction mappings, a minimum rate of convergence as being at least linear was also analytically established in [3, Theorem 5.2], *indicating a real-time capability* as verified in simulations by the small number of iterations

[8]Concepts which are similar to "controllable and observable," but slightly less restrictive [31].

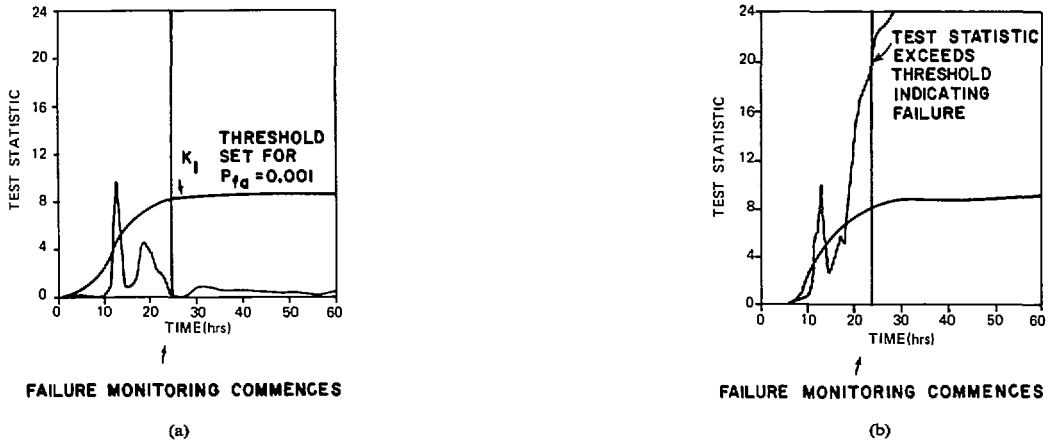

Fig. 3. INS (CR2) failure detection performance using real data. (a) No failure. (b) Large magnitude ramp drift rate failure in the equational input axis of a two degree of freedom gyro in an INS (SNR (24 h) = 5.38).

needed to converge. See [3] for more elaboration on aspects pertaining to rate of convergence.

The CR2[9] failure detection performance on real INS data for a naval application is presented in Fig. 3. Details of the 9-state reduced-order filter and 94-state truth model (used for superimposing failure responses) are omitted to avoid conflicts with classified national security information; however, a detailed structural block diagram is in [45]. When external position fixes are available to the INS, failures in the individual INS are more easily detected by a comparison to this more accurate external fix as a standard. The proposed use of the CR2 algorithm is to detect failures (of a certain critical magnitude corresponding to a certain critical signal-to-noise ratio associated with the resulting filter failure signal response to excessive gyro drift or accelerometer pickoff errors) between external fixes. The plot of Fig. 3(a) depicts the CR2 test statistic and the prespecified decision threshold K_1 under a no-failure condition using real data. After the initial 24 h[10], the test statistic is well below the decision threshold, confirming that no failure is present. The plot of Fig. 3(b) represents the CR2 test statistic and decision threshold for a simulated[11] large magnitude ramp drift-rate failure in one of the INS gyros. Following the initial 24 h waiting period, the CR2 test statistic quickly exceeds the threshold, correctly indicating a failure.

IV. An Intermediate Quantity Needed to Specify the Decision Threshold

A parameter $\bar{\lambda}$ is used in calculating the time-varying threshold for a specified probability of false alarm $P_{fa}(k)$, and in calculating the associated probability of correct detection $P_d(k)$. Using (11) and [33, Properties (6.2) and (6.28)], which relate an inner product to the trace of a matrix, the expected value of (25) is

$$E[l(\lambda,k)] = \lambda(1-\lambda)\mathrm{tr}[S(\lambda,k)] \tag{28}$$

where $S(\lambda,k)$ is just used for shortened notational convenience and is defined in (B.1-2) of Appendix B. By paralleling the steps of [3, pp. 518–519] that were used to obtain (26), but applying them to (28) instead, yields the value of λ that minimizes (28) as $\bar{\lambda}$. As obtained from the above step, the parameter $\bar{\lambda}$ is the solution of the following iteration equation[12]:

$$\bar{\lambda}_{n+1} = 1/\left[1+\left(\mathrm{tr}\left[\bar{A}^{-1}(\bar{\lambda}_n)\bar{P}_1(k)\bar{A}^{-1}(\bar{\lambda}_n)\right]/\mathrm{tr}\left[\bar{A}^{-1}(\bar{\lambda}_n)\right]\right)\right] \tag{29a}$$

$$= 1/\left[1+\left(\mathrm{tr}\left[S(\bar{\lambda}_n,k)P_1(k)A^{-1}(\bar{\lambda}_n)\right]/\mathrm{tr}\left[S(\bar{\lambda}_n,k)\right]\right)\right] \tag{29b}$$

with the initial value chosen (as explained in [3, Section 5]) such that

$$\frac{1}{2} < \bar{\lambda}_0 < 1 \tag{30}$$

where

$$\bar{A}(\bar{\lambda}_n) \triangleq [P_2-P_1]^{-1/2}A(\bar{\lambda}_n)[P_2-P_1]^{-1/2} \tag{31}$$

$$\bar{P}_1 \triangleq [P_2-P_1]^{-1/2}P_1[P_2-P_1]^{-1/2}. \tag{32}$$

The major steps in the proof of convergence of this scalar iteration equation parallel the almost identical steps that are used in the convergence proof that appears in [3, Theorem 5.2] for the other scalar iteration equation (26). Both equations have internal matrix structure of the same form [compare (26) to (29a)], but (26) becomes a scalar equation through the presence of inner products while (29) becomes a scalar equation through the presence of the trace operation.[13] The relevant steps of the proof of [3, Theorem 5.2] involve considering an associated underlying *matrix* equation of special structure from which convergence of the scalar equation (26) is inferred upon taking inner products. The same device of working with the associated matrix equation having the *same special structure* is sufficient to guarantee convergence of (29) by using an auxiliary result that relates the previous proof for inner products to a new proof for this case where the trace is used. The final step of the new convergence proof in converting the underlying matrix equation into a scalar equation is fulfilled by also taking specific inner products, and using the result of [33, eq. (6.8)] that now relates the required trace directly to these specific inner products as

$$\overset{(p\times p)}{\mathrm{tr}\,[U]} = \sum_{i=1}^{p} e_i^T U e_i$$

where e_i is a column vector consisting of all zeros except for a 1 in the ith position or row. As with (26), the conclusion is that (29) is a contraction. Expressions for the probabilities of false alarm and correct detection in terms of the intermediate quantity $\bar{\lambda}$ will now be obtained.

[9]CR2 is an acronym for two (2) confidence regions.

[10]The error dynamics of a gyro reflect the 24 h earth rotation rate; consequently, approximately one full 24 h period is required for the filter to lock onto the cycle of the underlying sinusoid. Initially, phase aligned *simulations* have no initial transient.

[11]Failure measurements were simulated from the official full-state error model of the form of (1) and (2) and superimposed in the real data using linearity. Cost of inducing actual failure in an INS would be prohibitive.

[12]Notice that this is a scalar iteration equation, just as (26) is, but that here internal matrix quantities are used in a trace.

[13]Stability in the sense of numerical analysts [37], which requires establishing continuity with respect to perturbations in the parameter matrices, is assured for both (26) and (29) since these iteration equations (used as successive approximations) have been demonstrated to be contraction mappings. Successive approximations with contraction mappings are guaranteed to be stable [37, p. 174].

V. Integral Expressions for P_{fa} and P_d at Each Check Time

Using the standard definitions of probability of false alarm and correct detection [5, p. 31] and applying them to the decision rule of (24), while using the underlying statistical structure of (8) and (9), yields the following expressions for these probabilities[14] at each check-time instant k, respectively, as

$$P_{fa}(k) \triangleq \text{Prob}[l(k) > K_1(k) | H_o] = \int_{l(k)>K_1(k)} \cdots \int N_{\hat{x}}(0, P_{\hat{x}\hat{x}}(k))\, d\hat{x} \quad (33a)$$

$$= \int_{\bar{\lambda}(1-\bar{\lambda})\hat{x}^T A^{-1}(\bar{\lambda})\hat{x} > K_1(k)} \cdots \int N_{\hat{x}}(0, P_{\hat{x}\hat{x}}(k))\, d\hat{x} \quad (33b)$$

$$P_d(k) \triangleq \text{Prob}[l(k) > K_1(k) | H_1] = \int_{l(k)>K_1(k)} \cdots \int N_{\hat{x}}(d(k), P_{\hat{x}\hat{x}}(k))\, d\hat{x} \quad (34a)$$

$$= \int_{\bar{\lambda}(1-\bar{\lambda})\hat{x}^T A^{-1}(\bar{\lambda})\hat{x} > K_1(k)} \cdots \int N_{\hat{x}}(d(k), P_{\hat{x}\hat{x}}(k))\, d\hat{x} \quad (34b)$$

where $d(k)$, as defined in (10), is the mean *deterministic* response of the filter to the specific failure $\bar{\nu}$ that is to be detected with the system and measurement noise sample functions zeroed out. The quantity $d(k)$ may be numerically quantified by simulating the specific failure ν in the failure mode of interest from the full state truth or error model of (1) and (2), with $Q(k)$ and $R(k)$ indentically zero, then processing the simulated failure measurements with the possibly reduced-order filter of (3)–(5) with $Q(k)$ and $R(k)$ at their proper nonzero design values.

The multidimensional signal-to-noise ratio (SNR) [7] that is used in evaluating $P_d(k)$ in (34) is

$$\text{SNR}(k) \triangleq \sqrt{d^T(k) P_{\hat{x}\hat{x}}(k)^{-1} d(k)} \quad (35)$$

[another convention is to define SNR as the square of (35)]. The objective of Sections VI and VII is the specification of a method whereby (33) and (34) may be explicitly evaluated. There is a natural dichotomy in the specification of a short easy solution for the scalar case (for two confidence intervals) and a more involved solution for the generalization to two multidimensional confidence regions (which will be completely detailed only for the representative two-dimensional case, since gyros have only one or two input axes).[15] *This dichotomy occurs because the optimization problem for the scalar case has a closed-form solution, as given in (20)–(22) to obtain the test statistic of (23), while the optimization for the multidimensional case involves use of the iterative algorithm of (26) to obtain the test statistic of (25).* Additionally, the multidimensional case requires the use of the iterative algorithm of (29) to determine the decision threshold with which the test statistic is compared in making failure/no-failure decisions as the decision rule of (24). The multidimensional Gaussian integral of (33) is solved for K_1 without recourse to CEP or SEP techniques [42], which would require eigenvector calculation by some additional iterative algorithm such as the Jacobi method [37], because the direct approach involving a matrix inversion appears to be more efficient.[16] Stability of this direct approach is established in Section VI, where conditions encountered in this application are summarized that guarantee convergence of the successive approximations procedure that is used to specify the decision threshold.

VI. Solving for the Decision Threshold

The objective of this section is to solve (33) for $K_1(k)$ when a prespecified value of $P_{fa}(k)$ is given as the requirement to meet.

Threshold for the Scalar Case: In the scalar case, both (26) and (29) reduce to

$$\bar{\lambda} = \lambda^* = \sqrt{P_2(k)} \,/\left(\sqrt{P_2(k)} + \sqrt{P_1(k)}\right) \quad (36)$$

and (33) may be simply represented, using (11), in terms of the well-tabulated error function as

$$P_{fa}(k) = \int_{\hat{x}_i^2 > K_1(k)\cdot\left(\sqrt{P_2}+\sqrt{P_1}\right)^2} N_{\hat{x}_i}(0, P_2(k) - P_1(k))\, d\hat{x}_i$$

$$= \int_{u^2 > K_1(k)\cdot\left(\sqrt{P_2}+\sqrt{P_1}\right)/\left[\left(\sqrt{P_2}-\sqrt{P_1}\right)^2\right]} e^{-u^2}/\sqrt{\pi}\, du \quad (37a)$$

$$= 1 - \frac{1}{2}\text{erf}\left[\sqrt{K_1(k)/2} \cdot \sqrt{\left(\sqrt{P_2(k)} + \sqrt{P_1(k)}\right)/\left(\sqrt{P_2(k)} - \sqrt{P_1(k)}\right)}\right]. \quad (37b)$$

To obtain the decision threshold $K_1(k)$, given a fixed value of instantaneous $P_{fa}(k)$ to be maintained at each check time, involves using tables to solve for the constant b in the following equation:

$$P_{fa}(k) = 1 - \frac{1}{2}\text{erf}\left[b/\sqrt{2}\right]. \quad (38)$$

Once b has been evaluated, this value of b may be equated to the argument of the error function of (37b) as

$$b/\sqrt{2} = \sqrt{K_1(k)/2} \cdot \sqrt{\left(\sqrt{P_2(k)} + \sqrt{P_1(k)}\right)/\left(\sqrt{P_2(k)} - \sqrt{P_1(k)}\right)} \quad (39a)$$

to be rearranged as the specification of the time-varying decision threshold $K_1(k)$ for the scalar case as

$$K_1(k) = b^2 \cdot \left[\left(\sqrt{P_2(k)} - \sqrt{P_1(k)}\right)/\left(\sqrt{P_2(k)} + \sqrt{P_1(k)}\right)\right]. \quad (39b)$$

Threshold for the Two-Dimensional Case: In the two-dimensional case, the solution of (33) for $K_1(k)$ requires a different route than the simple utilization of the tabulated error function that was available in the scalar case. The major intermediate steps in the evaluation of $K_1(k)$ for the two-dimensional case are summarized here as (40a)–(40i) to allow the main theme in the evaluation method to be perceived. *The underlying theoretical details that rigorously substantiate these intermediate steps are relegated to Appendix B.* The expression for the CR2 probability of false alarm, (33), may be reexpressed as

$$P_{fa}(k) = \int_{K_1(k)}^{\infty} p_{l|H_0}(l)\, dl = \int_{K_1}^{\infty} \left[\frac{1}{|a_1|} p_{\chi^2}\left(\frac{\cdot}{a_1}\right) * \frac{1}{|a_2|} p_{\chi^2}\left(\frac{\cdot}{a_2}\right)\right] dl \quad (40a)$$

$$= \int_{K_1}^{\infty} \left[\frac{\exp\{-l/2a_2\}}{2\pi\sqrt{a_1 a_2}} \int_0^l e^{-bx}/\sqrt{x(l-x)}\, dx\right] dl \quad (40b)$$

$$= \int_{K_1}^{\infty} \left[\left(1/4\pi\sqrt{a_1 a_2}\right) \int_{-\pi}^{\pi} \exp\left\{-\frac{1}{2}\left[\frac{1}{a_2} + b + b\sin\theta\right] l\right\} d\theta\right] dl \quad (40c)$$

$$= \left(1/4\pi\sqrt{a_1 a_2}\right) \int_{-\pi}^{\pi} \left[\int_{K_1}^{\infty} \exp\left\{-\frac{1}{2}\left[\frac{1}{a_2} + b + b\sin\theta\right] l\right\} dl\right] d\theta \quad (40d)$$

$$= \left(\exp\{-K_1 C/2\}/2\pi C\sqrt{a_1 a_2}\right) \int_{-\pi}^{\pi} \frac{\exp\{-(bK_1/2)\sin\theta\}}{1 + (b/C)\sin\theta}\, d\theta \quad (40e)$$

[14] Used $\bar{\lambda}(k)$ instead of $\lambda(k)$ to avoid measurement sample function (realization) dependence in an *a priori* evaluation.

[15] Accelerometer failures such as ramps or biases may also be detected by their effect on the gyro drift estimates without strict inclusion of additional accelerometer states in the model of (1).

[16] While eigenvalues are easy to calculate for the two-dimensional case, the two-dimensional matrices encountered in this INS application are also easily inverted analytically, thus facilitating an implementation of the CR2 technique.

$$= \left(\exp\{-K_1C/2\}/2\pi C\sqrt{a_1a_2}\right) \cdot \int_{-\pi}^{\pi}\left[\sum_{i=0}^{\infty}(-K_1b/2)^i(\sin\theta)^i/i!\right]/[1+(b/C)\sin\theta]\,d\theta \tag{40f}$$

$$= \left(\exp\{-K_1C/2\}/2\pi C\sqrt{a_1a_2}\right)\sum_{i=0}^{\infty}\left[(-K_1b/2)^i/i!\right] \cdot \int_{-\pi}^{\pi}(\sin\theta)^i/[1+(b/C)\sin\theta]\,d\theta \tag{40g}$$

$$= \left(\exp\{-K_1C/2\}/\pi C\sqrt{a_1a_2}\right)\sum_{i=0}^{\infty}\left[(K_1b)^i/i!\right] \cdot \int_{-\infty}^{\infty} z^i/\left[(z^2+2(b/C)z+1)(1+z^2)^i\right]dz \tag{40h}$$

$$= (\exp\{-K_1C/2\}/e_0)[e_0+e_1K_1+e_2K_1^2+e_3K_1^3+e_4K_1^4+e_5K_1^5+\cdots]. \tag{40i}$$

The final result being the algebraic series of (40i) which is devoid of all integral expressions and is just an algebraic equation to be solved for K_1. From manipulations of the matrix $S(\bar{\lambda}, k)$, defined in (B.1-2), the power series coefficients in (40i), obtained without having to solve for any *eigenvalues or eigenvectors*, are[17]

$$C \triangleq \mathrm{tr}\left[S(\bar{\lambda},k)\right]/\left[2\bar{\lambda}(1-\bar{\lambda})\det\left[S(\bar{\lambda},k)\right]\right] > 0 \tag{41}$$

$$b^2 \triangleq \left(\mathrm{tr}\left[S(\bar{\lambda},k)S(\bar{\lambda},k)\right]-2\det\left[S(\bar{\lambda},k)\right]\right)/\left[2\bar{\lambda}(1-\bar{\lambda})\right]^2 > 0 \tag{42}$$

$$e_0 \triangleq \mathrm{tr}\left[S(\bar{\lambda},k)\right]/2\sqrt{\det\left[S(\bar{\lambda},k)\right]} > 0 \tag{43}$$

$$e_1 \triangleq \frac{C}{2}[e_0-1] \tag{44a}$$

$$e_2 \triangleq \frac{1}{2}\left(\frac{C}{2}\right)e_1 \tag{44b}$$

$$e_3 \triangleq \frac{1}{3}\left(\frac{C}{2}\right)\left[e_2-\frac{b^2}{2^4}\right] \tag{44c}$$

$$e_4 \triangleq \frac{1}{4}\left(\frac{C}{2}\right)e_3 \tag{44d}$$

$$e_5 \triangleq \frac{1}{5}\left(\frac{C}{2}\right)\left[e_4-\frac{(b^2)^2}{2^{10}}\right]. \tag{44e}$$

When $\bar{\lambda}, P_1(k)$, and $P_2(k)$ are known, then $S(\bar{\lambda}, k)$ of (B.1-2) is specified; therefore, by (41)–(44), all the coefficients can be calculated. For a given desired $P_{fa}(k)$, all that remains to be done is to solve the nonlinear equation, (40i), for the unknown $K_1(k)$. This is achieved by using a successive approximations approach [37] in conjunction with the following device.

When rearranged, (40i) becomes the following nonlinear algebraic equation:

$$e_0 \cdot P_{fa}(k) \cdot \exp[K_1 \cdot C/2] = e_0+e_1K_1+e_2K_1^2+e_3K_1^3+e_4K_1^4+e_5K_1^5 \tag{45}$$

that must be solved for $K_1(k)$ at each check time k. Let

$$y_1(K_1) \triangleq e_0+e_1K_1+e_2K_1^2+e_3K_1^3+e_4K_1^4+e_5K_1^5 \tag{46}$$

$$y_2(K_1) \triangleq e_0 \cdot P_{fa}(k) \cdot \exp[K_1C/2]. \tag{47}$$

If y_1 versus K_1 is plotted using (46) and if y_2 versus K_1 is plotted using (47), as shown in Fig. 4, then the positive K_1 value where the two graphs intersect is the value K_1 that is a solution of (45) and, equivalently of (40). All the coefficients of the polynomial of (46) are positive (Proposition 1 of Appendix B); hence the quintic y_1 is monotone increasing for positive K_1. The vertical asymptote of the quintic y_1 is e_0; since

$$0 < P_{fa}(k) < 1 \tag{48}$$

the increasing exponential y_2 has a vertical asymptote, $e_0 \cdot P_{fa}(k)$, which is below the vertical asymptote of the quintic y_1. Even though y_2 starts below y_1, the fact that an increasing exponential will always asymptotically dominate a polynomial guarantees that these two curves will indeed intersect at one point and, therefore, that a unique positive solution $\bar{K}_1$ will always exist. This point $\bar{K}_1$ may be found by the successive approximations procedure as illustrated in Fig. 4. *For this application to the exponential that is dominated near zero by the quintic polynomial with all coefficients positive, the successive approximations procedure always converges* so there are no numerical difficulties when computer evaluation is used.

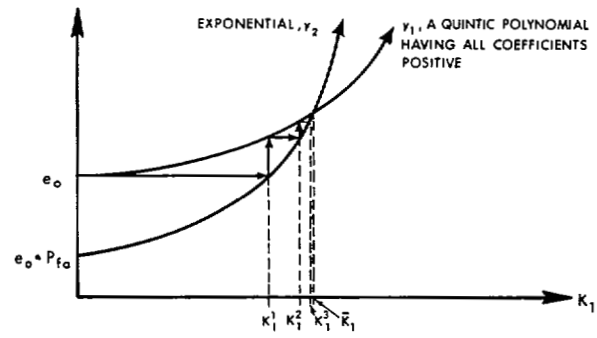

Fig. 4. Successive approximations solution of K_1.

Time-varying decision thresholds, precalculated according to the above procedure and used in conjunction with the two-dimensional CR2 test statistic to detect failures in the real data of Fig. 3, are shown in Fig. 5 for a range of probability of false alarm. These thresholds are exact and are below the upper bounds obtained from the asymptotic, as time increases, χ^2_2 distribution of the l-statistic [See (40a)].

VII. Calculating the Instantaneous Probability of Correct Detection that Corresponds to the Threshold Setting

Given that $\bar{\lambda}$, $P_1(k)$, and $P_2(k)$ are known (from (29), (4), and (7), respectively) and that the threshold $\bar{K}_1(k)$ corresponding to a given specified $P_{fa}(k)$ has been previously determined (as discussed in Section VI), it is desired that $P_d(k)$ of (34) be evaluated so that the likelihood of detecting a specific failure mode $\bar{\nu}$, when it occurs, is quantified.

$P_d(k)$ for the Scalar Case

Again the Lagrange multiplier $\bar{\lambda}$, necessary for evaluating (34), is given by (36) for the scalar case. Using (36) for $\bar{\lambda}$, the expression of (34) reduces to

$$P_d(k) = 1-\frac{1}{2}\mathrm{erf}\left[\left(\mathrm{SNR}(k)/\sqrt{2}\right)+\sqrt{K_1(k)/2} \cdot \sqrt{\left(\sqrt{P_2(k)}+\sqrt{P_1(k)}\right)/\left(\sqrt{P_2(k)}-\sqrt{P_1(k)}\right)}\right] - \frac{1}{2}\mathrm{erf}\left[\left(\mathrm{SNR}(k)/\sqrt{2}\right)-\sqrt{K_1(k)/2} \cdot \sqrt{\left(\sqrt{P_2(k)}+\sqrt{P_1(k)}\right)/\left(\sqrt{P_2(k)}-\sqrt{P_1(k)}\right)}\right] \tag{49}$$

where, for the scalar case, the expression for the signal-to-noise ratio of (35) simplifies as

$$\mathrm{SNR}(k) = |d(k)|/\sqrt{P_2(k)-P_1(k)}\,. \tag{50}$$

All the terms in the argument of the error functions of (49) are known so that it may be numerically evaluated.

$P_d(k)$ for the Two-Dimensional Vector Case

Equation (34) may be rewritten for two dimensions via a coordinate (i.e., similarity) transformation as

[17]Notice that the coefficients e_1, e_2, e_3, e_4, and e_5 are completely defined in terms of e_0, b^2, and C.

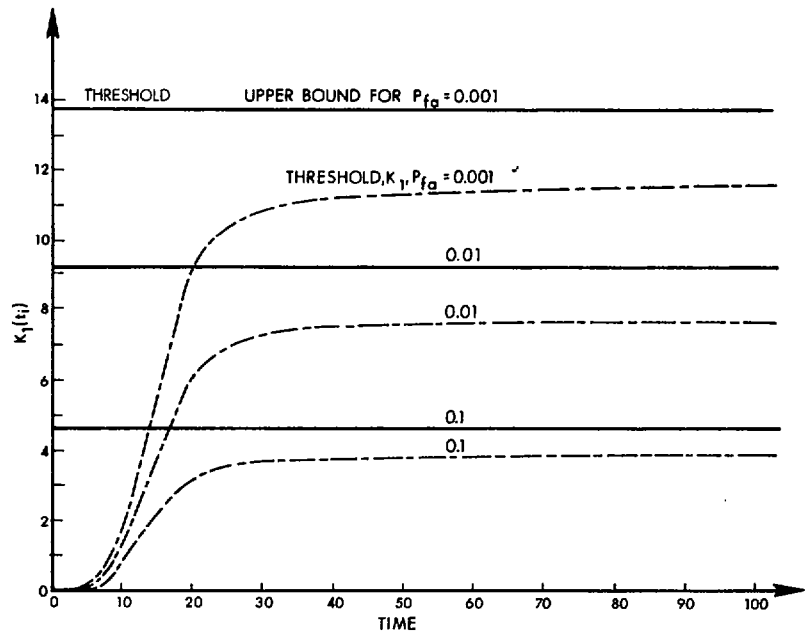

Fig. 5. Time-varying threshold used for two-dimensional CR2.

$$P_d(k) = 1 - \iint_G N_u(0, I)\, du \tag{51}$$

where G is the following region:

$$\left(u + [P_2 - P_1]^{-1/2} d(k)\right)^T \bar{A}^{-1}(\bar{\lambda})\left(u + [P_2 - P_1]^{-1/2} d(k)\right) \leq \frac{\bar{K}_1(k)}{\bar{\lambda}(1-\bar{\lambda})} \tag{52}$$

where the integral represents the volume under the circular Gaussian surface enclosed by the ellipse as illustrated in Fig. 6.

Using the definition of the multidimensional signal-to-noise ratio in (35), the integral of (51), represented in Fig. 6, may be closely approximated by the integral represented in Fig. 7 by applying the cyclic property of the trace operation [33, eq. (6.14)] on the definition of (31) to yield

$$\operatorname{tr}\left[\bar{A}^{-1}(\bar{\lambda})\right] = \operatorname{tr}\left[S(\bar{\lambda}, k)\right]. \tag{53}$$

Consequently, the intermediate quantity R^2 may be obtained from (52) as

$$R^2 \triangleq \bar{K}_1(k) / \left[\bar{\lambda}(1-\bar{\lambda}) \operatorname{tr}\left[S(\bar{\lambda}, k)\right]\right]. \tag{54}$$

This quantity R is an input entry along with

$$D \triangleq \mathrm{SNR}(k)$$

which are both used in the tables of [40] to enable the readout of the numerical quantification of "offset circle probabilities for the circular normal distribution" of Fig. 7 as an easily accessible approximation to the evaluation of (51). The exact evaluation of (51) is in [41]. Now that the expressions provided by this paper are available for P_{fa} and P_d for a particular failure ν, the Bayes, Neyman–Pearson, or minimax criteria [6] can be used in a tradeoff to specify the setting of the decision threshold level scaling parameter b that appears in (39b) (for the scalar case) or to specify setting of the explicit threshold scaling parameter P_{fa} that appears in (45) and (47).

While all of the results of the CR2 statistical analysis and threshold setting of Sections VI and VII have been obtained under the assumption of an optimal Kalman filter in (3)–(5) of the same dimension as the system model of (1), (2), the CR2 results pertaining to test statistic calculation, to threshold setting, and to statistical analysis of the decisions remain valid when a reduced-order filter formulation, such as [25] or [26] is used. The reduced-order filter approaches of [25] and [26] still yield the *correct covariance and cross correlations associated with the reduced-order filter*. The same Gaussian random processes are inputs to the reduced-order filter; therefore, the outputs are also Gaussian processes since the reduced-order filter, although not optimal, is still a linear system and consequently supplies all the information needed—namely, the means and variances—for a fully rigorous interpretation of the resulting two confidence regions.

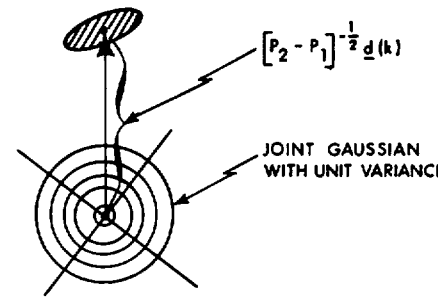

Fig. 6. Shaded area encloses volume represented by integral in (51).

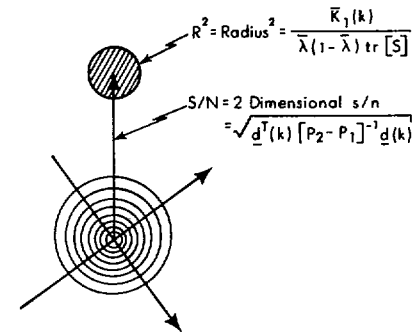

Fig. 7. Circle approximation used in $P_d(k)$ calculation.

VIII. Summary

The two confidence region (CR2) approach to failure detection is revealed in Section II to be a generalization to two or more dimensions of a simpler noniterative two-confidence interval failure detection approach. The advantage of generalization is illustrated in the application of the two-dimensional CR2 in detecting subtle out of tolerance drift-rate "failures," between external position resets, in a two-degree-of-freedom gyro within an inertial navigation system. It is shown in Appendix A that the two-dimensional CR2 failure detection approach does not discard the information on the skewness or tilt of the underlying ellipsoids contained in the cross correlations and actually utilizes a greater (or equal in a worse case situation) input signal-to-noise ratio than would be utilized by two uncorrelated simultaneous one-dimensional detectors. (The same conclusion trivially holds for an n-dimensional CR2 versus n uncorrelated one-dimensional detectors.)

The equations and evaluation procedure for an off-line statistical analysis of the decision test, as derived here, in conjunction with the rigorous proof of convergence and convergence rate in [3] (summarized in Section III), and the refinement for evaluating the probability of false alarm over a time interval [43] should provide a complete view of the CR2 approach to failure detection. The performance of the CR2 approach in detecting gyro drift-rate failures in an inertial navigation system is demonstrated in Section III using real data. A conventional discrete-state Markov reliability/availability analysis of the effect of failure detection on the overall performance of a complex navigation system, using the standard reliability techniques of [44], is provided in [45].

Appendix A
An Advantage of One Two-Dimensional CR2 Failure Detector Over Two One-Dimensional Detectors

The definition of signal-to-noise ratio (SNR) of (35) may be expanded for the two-dimensional case as

$$\mathrm{SNR}_2(k)=\sqrt{\frac{1}{(1-\rho^2)}\left[\left(\frac{d_1}{\sigma_1}\right)^2-2\rho\left(\frac{d_1}{\sigma_1}\right)\left(\frac{d_2}{\sigma_2}\right)+\left(\frac{d_2}{\sigma_2}\right)^2\right]} \quad \text{(A.1)}$$

and the two associated one-dimensional scalar signal-to-noise ratios for each subcomponent are

$$\mathrm{SNR}_1 \triangleq |d_1|/\sigma_1 \quad \text{(A.2)}$$

and

$$\mathrm{SNR}_{1'} \triangleq |d_2|/\sigma_2. \quad \text{(A.3)}$$

Theorem 1: For a strict inequality on the correlation coefficient of

$$-1<\rho<1 \quad \text{(A.4)}$$

and with

$$d_j \neq (\rho\sigma_j/\sigma_i)\,d_i \qquad \text{for } i\neq j, \quad \text{(A.5)}$$

then

$$\mathrm{SNR}_2 > \mathrm{SNR}_1 \quad \text{(A.6)}$$

and

$$\mathrm{SNR}_2 > \mathrm{SNR}_{1'}. \quad \text{(A.7)}$$

Proof: The following is nonnegative because it is a squared quantity, and nonzero because of the condition of (A.5):

$$\left[(d_j/\sigma_j)-\rho(d_i/\sigma_i)\right]^2>0 \qquad \text{for } j\neq i. \quad \text{(A.8)}$$

Expanding (A.8) yields

$$(d_j/\sigma_j)^2-2\rho(d_j/\sigma_j)(d_i/\sigma_i)+\rho^2(d_i/\sigma_i)^2>0 \quad \text{(A.9)}$$

which, upon rearranging, becomes

$$(d_j/\sigma_j)^2-2(d_j/\sigma_j)(d_i/\sigma_i)>-\rho^2(d_i/\sigma_i)^2 \qquad \text{for } i\neq j. \quad \text{(A.10)}$$

Now adding the nonnegative quantity $(d_i/\sigma_i)^2$ to both sides of (A.10) yields

$$(d_j/\sigma_j)^2-2\rho(d_j/\sigma_j)(d_i/\sigma_i)+(d_i/\sigma_i)^2>(1-\rho^2)(d_i/\sigma_i)^2 \qquad \text{for } i\neq j. \quad \text{(A.11)}$$

From the condition of (A.4), it occurs that

$$0\leq\rho^2<1 \quad \text{(A.12)}$$

and, by subtraction, the following result is obtained:

$$1\geq 1-\rho^2>0. \quad \text{(A.13)}$$

Dividing through (A.11) by the strictly positive quantity of (A.13), yields

$$\frac{1}{(1-\rho^2)}\left[(d_j/\sigma_j)^2-2\rho(d_j/\sigma_j)(d_i/\sigma_i)+(d_i/\sigma_i)^2\right]>(d_i/\sigma_i)^2 \quad \text{(A.14)}$$

which, upon taking square roots of both sides, yields the conclusions of (A.6) and (A.7) for $i=1$ and $i=2$, respectively. ∎

Comment 1: Theorem 1 states that because of the cross correlation information the SNR provided as an input to the two-dimensional failure detection implementation is greater than that provided to both subcomponent scalar failure detection implementations. Numerical quantification indicates that the advantage is sometimes greater than the square-root of the sum of the squares of both the subcomponent SNR's.

Comment 2: The conclusion of Theorem 1 as (A.6), (A.7) may be jointly summarized as $\mathrm{SNR}_2>\max(\mathrm{SNR}_1,\mathrm{SNR}_1')$.

Comment 3: Upon removing the restriction of (A.5), the conclusion of Theorem 1 as (A.6), (A.7) must be weakened to allow possible equality.

Appendix B
Details of the Threshold Calculation for the Vector Case (Dimension: 2)

The underlying mathematical analysis sketched in Section VI to emphasize the end objective of solving (40) for $K_1(k)$ is now presented in logical order with the steps being formulated as propositions, lemmas,[18] a corollary, and a theorem. Appendix B.1 consists of the proper statements of what is to be proved. Appendix B.2 consists of sketches of the proofs.

B.1 Statements to be Proved

Lemma 1: The characteristic function for $l(\bar{\lambda},k)$ of (25) under H_0 for the *general multidimensional* case is

$$\phi_l(\nu,\bar{\lambda},k)\triangleq E\left[e^{jl(k)\nu}\,|\,H_0\right]$$

$$=E\left[e^{j\nu\bar{\lambda}(1-\bar{\lambda})\tilde{x}^T(k)\mathcal{A}^{-1}(k)\tilde{x}(k)\nu}\,|\,H_0\right] \quad \text{(B.1-1a)}$$

$$=|P_2(k)-P_1(k)|^{-1/2}$$

$$\cdot\left|[P_2(k)-P_1(k)]^{-1}-j2\nu\bar{\lambda}(1-\bar{\lambda})\left[(1-\bar{\lambda})P_2(k)+\bar{\lambda}P_1(k)\right]^{-1}\right|^{-1/2} \quad \text{(B.1-1b)}$$

$$=\left|\left[I-j2\nu\bar{\lambda}(1-\bar{\lambda})[P_2(k)-P_1(k)]\left[(1-\bar{\lambda})P_2(k)+\bar{\lambda}P_1(k)\right]^{-1}\right]^{-1}\right|^{1/2} \quad \text{(B.1-1c)}$$

$$=\left|\left[1-j2\nu\bar{\lambda}(1-\bar{\lambda})S(\bar{\lambda},k)\right]^{-1}\right|^{1/2} \quad \text{(B.1-1d)}$$

[18] Only Lemma 1 holds without modification for the general multidimensional case. Extensions of Corollary 1, Theorem 2, and Propositions 1 and 2 to the general n dimensional case is still open since the intended application reported in Section III required only scalar and two-dimensional results. However, calculation of the test statistic [via (25), (26)], calculation of the auxiliary quantity λ [via (29)], and the convergence guarantee of [3] are valid for arbitrary dimensions.

$$= \left| \left[I - j2\nu\bar{\lambda}(1-\bar{\lambda}) V(k) \left[P_2(k) - \bar{\lambda}[P_2(k) - P_1(k)] \right]^{-1} V^T(k) \right]^{-1} \right|^{1/2} \tag{B.1-1e}$$

$$= \left| \left[I - j2\nu\bar{\lambda}(1-\bar{\lambda}) \left[V^{-T}(k) P_2(k) V^{-1}(k) - \bar{\lambda} I \right]^{-1} \right]^{-1} \right|^{1/2} \tag{B.1-1f}$$

$$= \left| \left[I - j2\nu\bar{\lambda}(1-\bar{\lambda}) \left[M(k) - \bar{\lambda} I \right]^{-1} \right]^{-1} \right|^{1/2} \tag{B.1-1g}$$

$$= |U^{-1}(k)|^{1/2} \cdot \left| \left[I - j2\nu\bar{\lambda}(1-\bar{\lambda}) \left[M(k) - \bar{\lambda} I \right]^{-1} \right]^{-1} \right|^{1/2} \cdot |U(k)|^{1/2} \tag{B.1-1h}$$

$$= \left| \left[I - j2\nu\bar{\lambda}(1-\bar{\lambda}) \left[U^{-1}(k) M(k) U(k) - \bar{\lambda} I \right]^{-1} \right]^{-1} \right|^{1/2} \tag{B.1-1i}$$

$$= \left| \left[I - j2\nu\bar{\lambda}(1-\bar{\lambda}) \left[\Lambda(k) - \bar{\lambda} I \right]^{-1} \right]^{-1} \right|^{1/2} \tag{B.1-1j}$$

$$= \left| \left[I - j2\nu\bar{\lambda}(1-\bar{\lambda}) \left[\{ d_{ii}(k) - \bar{\lambda} \}_{i=1}^{P} \right]^{-1} \right]^{-1} \right|^{1/2} \tag{B.1-1k}$$

$$= \left| \left[\left\{ 1 - \left(j2\nu\bar{\lambda}(1-\bar{\lambda}) / \left(d_{ii}(k) - \bar{\lambda} \right) \right) \right\}_{i=1}^{P} \right]^{-1} \right|^{1/2} \tag{B.1-1l}$$

$$= \prod_{i=1}^{P} \left(1 - \left(j2\nu\bar{\lambda}(1-\bar{\lambda}) / \left(d_{ii}(k) - \bar{\lambda} \right) \right) \right)^{-1/2} \tag{B.1-1m}$$

where, in the above,

$$S(\bar{\lambda}, k) \triangleq [P_2(k) - P_1(k)] \left[(1-\bar{\lambda}) P_2(k) + \bar{\lambda} P_1(k) \right]^{-1} \tag{B.1-2}$$

and

$$[P_2(k) - P_1(k)] = V^T(k) V(k) \tag{B.1-3}$$

where (B.1-3) results from a Choleski factorization [37] and

$$M(k) = V^{-T}(k) P_2(k) V^{-1}(k) \tag{B.1-4}$$

where $U(k)$ is the normalized eigenvector matrix[19] associated with the symmetric matrix $M(k)$, therefore using $U(k)$ in a similarity transformation diagonalizes $M(k)$ as

$$U^{-1}(k) M(k) U(k) = \Lambda(k) = \operatorname{diag}(d_{11}(k), d_{22}(k), \cdots, d_{pp}(k)) \tag{B.1-5}$$

with

$$|S^{-1}(\bar{\lambda}, k)| = |M - \bar{\lambda} I| = |\Lambda - \bar{\lambda} I| = \prod_{i-1}^{P} \left(d_{ii}(k) - \bar{\lambda} \right) \tag{B.1-6}$$

$$\operatorname{tr}\left[S^{-1}(\bar{\lambda}, k) \right] = \operatorname{tr}[M - \bar{\lambda} I] = \operatorname{tr}[\Lambda - \bar{\lambda} I] = \sum_{i=1}^{P} \left(d_{ii}(k) - \bar{\lambda} \right). \tag{B.1-7}$$

Equation (B.1-1m) is recognized to be the product of the characteristic functions of weighted chi-square random variables [38] which represents the sum of weighted independent chi-squared random variables [39, eq. 7-7] and has the following probability density function:

$$p_{l(k)|H_0^{(1)}} = \frac{1}{|a_1|} p_{\chi_1^2}\left(\frac{\cdot}{a_1} \right) * \frac{1}{|a_2|} p_{\chi_1^2}\left(\frac{\cdot}{a_2} \right) * \cdots * \frac{1}{|a_p|} p_{\chi_1^2}\left(\frac{\cdot}{a_p} \right) \tag{B.1-8}$$

where

$$a_i(k) \triangleq \bar{\lambda}(1-\bar{\lambda}) / \left(d_{ii}(k) - \bar{\lambda} \right) > 0 \qquad \text{for } (i = 1, \cdots, p) \tag{B.1-9}$$

and $*$ represents convolution.

Corollary 1: For the two-dimensional case, (B.1-8) becomes

$$p_{\substack{l(k)|H_0 \\ p=2}}(\omega) = \frac{1}{a_1} p_{\chi_1^2}\left(\frac{\cdot}{a_1} \right) * \frac{1}{a_2} p_{\chi_1^2}\left(\frac{\cdot}{a_2} \right) \tag{B.1-10a}$$

$$= \left(1/4\pi\sqrt{a_1 a_2} \right) \int_{-\pi}^{\pi} \exp\left\{ -\frac{1}{2} \left[\frac{1}{a_2} + b + b\sin\Theta \right] \omega \right\} d\Theta \tag{B.1-10b}$$

thus establishing (40a), (40b), and (40c), where

$$b \triangleq (a_2 - a_1)/2a_2 a_1. \tag{B.1-11}$$

Theorem 2: For the two-dimensional case, use of the results of (B.1-10) allows (33) to be evaluated as shown in each of the intermediate steps of (40), where

$$C \triangleq \frac{1}{a_2} + b = \frac{1}{a_2} + \frac{a_2 - a_1}{2a_2 a_1} = \frac{a_2 + a_1}{2a_2 a_2} > 0. \tag{B.1-12}$$

Proposition 1: By the inequality of (B.1-9) and the definitions of b and C in (B.1-11) and (B.1-12), it follows that

$$0 < (b/C)^2 < 1 \tag{B.1-13}$$

and therefore that

$$0 < e_i \qquad i = 0, \cdots, 5. \tag{B.1-14}$$

Proposition 2: The following identities are used to evaluate the coefficients of (41)–(44) while avoiding any explicit eigenvalue evaluation:

$$a_1 a_2 = \bar{\lambda}^2 (1-\bar{\lambda})^2 / \det\left[S^{-1}(\bar{\lambda}, k) \right] \tag{B.1-15}$$

$$a_1 + a_2 = \bar{\lambda}(1-\bar{\lambda}) \operatorname{tr}\left[S^{-1}(\bar{\lambda}, k) \right] / \det\left[S^{-1}(\bar{\lambda}, k) \right] \tag{B.1-16}$$

$$C = (a_2 + a_1)/2a_1 a_2 = \operatorname{tr}\left[S^{-1}(\bar{\lambda}, k) \right] / \left(2\bar{\lambda}(1-\bar{\lambda}) \right) \tag{B.1-17}$$

$$e_0 = 1/\sqrt{1 - (b/C)^2} = (a_2 + a_1)/2\sqrt{a_1 a_2}$$

$$= \operatorname{tr}\left[S^{-1}(\bar{\lambda}, k) \right] / 2\sqrt{\det\left[S^{-1}(\bar{\lambda}, k) \right]} \tag{B.1-18}$$

$$\sqrt{a_1 a_2}\, C = \operatorname{tr}\left[S^{-1}(\bar{\lambda}, k) \right] / 2\sqrt{\det\left[S^{-1}(\bar{\lambda}, k) \right]} \tag{B.1-19}$$

$$a_2^2 + a_1^2 = \bar{\lambda}^2 (1-\bar{\lambda})^2 \operatorname{tr}\left[S^{-1}(\bar{\lambda}, k) \cdot S^{-1}(\bar{\lambda}, k) \right] / \det\left[S^{-1}(\bar{\lambda}, k) \right]^2 \tag{B.1-20}$$

$$b^2 = (a_2 - a_1)^2 / (2a_1 a_2)^2 = (a_2^2 + a_1^2 - 2a_1 a_2) / (2a_1 a_2)^2 \tag{B.1-21a}$$

$$= \left(\operatorname{tr}\left[S^{-1}(\bar{\lambda}, k) \cdot S^{-1}(\bar{\lambda}, k) \right] - 2\det\left[S^{-1}(\bar{\lambda}, k) \right] \right) / \left(4\bar{\lambda}^2 (1-\bar{\lambda})^2 \right) \tag{B.1-21b}$$

where $S(\bar{\lambda}, k)$ is defined in (B.1-2).

B.2. Proofs

Proof of Lemma 1: Equation (B.1-1a) results from the definition of the characteristic function. Equation (B.1-1b) results when the definition of expectation is used in (B.1-1a), i.e.,

$$E\left[e^{j\bar{\lambda}(1-\bar{\lambda}) \hat{x}^T(k) A^{-1}(k) \hat{x}(k) \nu} \middle| H_0 \right]$$

$$\triangleq \int \cdots \int \exp\left\{ j\bar{\lambda}(1-\bar{\lambda}) \hat{x}^T A^{-1} \hat{x} \nu - \frac{1}{2} \hat{x}^T [P_2 - P_1]^{-1} \hat{x} \right\}$$

$$\cdot (2\pi)^{-P/2} |P_2 - P_1|^{-1/2} d\hat{x} \tag{B.2-1a}$$

$$= |P_2 - P_1|^{-1/2} |Q(\bar{\lambda}, \nu)|^{-1/2} \int \cdots \int (2\pi)^{-P/2} |Q(\bar{\lambda}, \nu)|^{1/2}$$

$$\cdot \exp\left\{ -\frac{1}{2} \hat{x}^T Q(\bar{\lambda}, \nu) \hat{x} \right\} d\hat{x} \tag{B.2-1b}$$

$$= |P_2 - P_1|^{-1/2} |Q(\bar{\lambda}, \nu)|^{-1/2} \tag{B.2-1c}$$

where

$$Q(\lambda, \nu) = [P_2 - P_1]^{-1} - j2\bar{\lambda}(1-\bar{\lambda}) A^{-1}(\bar{\lambda}) \nu. \tag{B.2-2}$$

[19] Eigenvalues, eigenvectors, and matrix factorizations are not actually calculated; they are used here for a theoretical examination of the problem structure.

Equation (B.1-1c) follows from (B.1-1b) since the determinant of the product of two matrices is the product of their determinants. Equation (B.1-1d)–(B.1-1g) are self-explanatory and reflect different groupings or observations about the internal structure. Equations (B.1-1h), (B.1-1i), and (B.1-1j) follow since the determinant is invariant under a similarity transformation. Equations (B.1-1k), (B.1-1ℓ), and (B.1-1m) result from the characteristically convenient manipulations that can be performed with diagonal matrices. ■

Proof of Corollary 1: Writing the convolution of (B.1-8) explicitly for the two-dimensional case yields

$$p_{\underline{b}=2}(\omega)=\frac{e^{-\omega/2a_2}}{\sqrt{a_1a_2}\,2\pi}\int_0^{\omega}\frac{1}{\sqrt{x(\omega-x)}}e^{-bx}dx \tag{B.2-3}$$

where the summarizing notation of (B.1-11) for b has been used. Completing the square of the denominator term under the radical in the integrand of (B.2-3) and using the following trigonometric substitution [36] $x-(\omega/2)=(\omega\sin\theta)/2$ yields

$$p_{\underline{b}=2}(\omega)=\left(1/4\pi\sqrt{a_1a_2}\right)\int_{-\pi/2}^{+\pi/2}\exp\left\{-\frac{1}{2}\left[\frac{1}{a_2}+b+b\sin\theta\right]\omega\right\}d\theta. \tag{B.2-4}$$

For the integrand of (B.2-4),

$$\int_{-\pi}^{+\pi}=2\int_{-\pi/2}^{\pi/2}; \tag{B.2-5}$$

therefore, using (B.2-5) in (B.2-4) yields (B.1-10b). ■

Proof of Theorem 2: Since the integrand of (B.1-10b) is positive and (B.1-10a) is a pdf and, as such, has a finite integral when integrated over K_1 to ∞, use of Fubini's theorem [34] allows the rigorous interchange of the order of integration, resulting in (40e). Equation (40e) may be rewritten, using the series expansion of the exponential, as (40f). Since the resulting series of continuous functions in (40f) *is a uniformly convergent series* by the Weierstrass M-test [35], the order of integration and summation can be rigorously (i.e., validly) interchanged in (40f) to result in (40g). Using the half-angle substitution [36] of $z=\tan(\theta/2)$ in (40g) yields (40h).

The real integrals of (40h) may be evaluated using Cauchy's residue theorem [34] in conjunction with some limiting arguments about how the complex extension of the real integrals of (40h) have zero contribution over the infinite semicircle in the upper half of the complex plane. The general integral of (40h) has poles where

$$z^2+2(b/C)z+1=0 \tag{B.2-6}$$

and where

$$z^2+1=0. \tag{B.2-7}$$

Since (B.2-6) is a quadratic equation, the poles enclosed by the closed contour in the upper half-plane are

$$z=-\frac{b}{C}+j\sqrt{1-(b/C)^2}\quad\text{and}\quad z=+_j1\quad\text{(of multiciplicity } i\text{)}. \tag{B.2-8}$$

Evaluating the first six terms in the series of (40h) using Cauchy's residue theorem (in the manner described above), results in (40i) [with coefficients defined as in Eqs. (41)–(44)]. ■

Proof of Proposition 1: Using the definition of (B.1-9), (B.1-11), and (B.1-12)

$$\begin{aligned}0<(b/C)^2&=((a_2-a_1)/(2a_1a_2))^2/((a_2+a_1)/(2a_1a_2))^2\\&=(a_2-a_1)^2/(a_2+a_1)^2<1.\end{aligned} \tag{B.2-9}$$

Now (B.2-9) implies that

$$1>1-(b/C)^2>0 \tag{B.2-10}$$

and, consequently, that

$$1/\sqrt{1-(b/C)^2}>1; \tag{B.2-11}$$

hence,

$$e_0=1/\sqrt{1-(b/C)^2}>1>0 \tag{B.2-12}$$

and

$$e_1=(C/2)[e_0-1]>0 \tag{B.2-13}$$

since $(C/2)$ is positive by (B.1-12) and (B.1-17). Also

$$e_2=(C/2)e_1>0. \tag{B.2-14}$$

Since e_3 through e_5 may be represented in an expanded form, e.g.,

$$e_3=\frac{1}{3}(C/2)\left[\left\{(C/2)^2/\sqrt{1-(b/C)^2}\right\}-(C/2)^2-(b^2/2^3)\right], \tag{B.2-15}$$

these remaining coefficients may be similarly demonstrated to be positive. ■

Proof of Proposition 2: Results follow using simple algebra and the definition of a_i, $S(\bar{\lambda},k)$, the trace and determinant as the sum and product of eigenvalues, respectively. ■

References

[1] T. H. Kerr, "A two ellipsoid overlap test for real-time failure detection and isolation by confidence regions," in *Proc. 5th Ann. Pittsburgh Conf. Modeling and Simulation*, part 2, 1974, p. 1003.

[2] ——, "A two ellipsoid overlap test for real-time failure detection and isolation by confidence regions," in *Proc. Conf. Decision Contr.*, 1974, pp. 735–742.

[3] ——, "Real-time failure detection: A static nonlinear optimization problem that yields a two ellipsoid overlap test," *J. Optimiz. Theory Appl.*, vol. 22, Aug. 1977.

[4] D. J. Sakrison, *Notes on Analog Communication*. New York: Van Nostrand Reinhold, 1970.

[5] H. L. Van Trees, *Detection, Estimation and Modulation Theory: Part I*. New York: Wiley, 1968.

[6] I. Selin, *Detection Theory*. Princeton, NJ: Princeton Univ. Press, 1965.

[7] C. H. Helstrom, *Statistical Theory of Signal Detection*. New York: Pergamon, 1968.

[8] A. S. Willsky, "A survey of design methods for failure detection in dynamic systems," *Automatica*, vol. 12, Nov. 1976.

[9] R. A. Nash *et al.*, "Application of optimal smoothing to the testing and evaluation of inertial navigation systems and components," *IEEE Trans. Automat. Contr.*, vol. AC-16, Dec. 1971.

[10] H. Rome, "Automated degradation detection and isolation for SINS," in *Proc. AIAA Guidance and Control Conf.*, Key Biscayne, FL, Aug. 1973.

[11] J. J. Deyst and J. C. Deckert, "Application of likelihood ratio methods to failure detection and identification in the NASA F-8 DFBW aircraft," in *Proc. Conf. Decision Contr.*, Houston, TX, Dec. 1975.

[12] J. C. Deckert, M. N. Desai *et al.*, "F8-DFBW sensor failure identification using analytic redundancy," *IEEE Trans. Automat. Contr.*, vol. AC-22, Oct. 1977.

[13] J. V. Harrison and T. T. Chien, "Failure isolation for a minimally redundant inertial sensor system," *IEEE Trans. Aerospace Electron. Syst.*, vol. AES-11, May 1975.

[14] T. T. Chien and M. B. Adams, "A sequential failure detection technique and its application," *IEEE Trans. Automat. Contr.*, vol. AC-21, Oct. 1976.

[15] R. Montgomery, "Failure detection and control system reconfiguration," presented at the MIT-NASA/AMES Workshop on Systems Reliability Issues for Future Aircraft, Mass. Inst. Technol., Cambridge, MA, Aug. 18–22, 1975.

[16] R. B. Broen, "Performance of fault tolerant estimators in a noisy environment," in *Proc. AIAA Guidance Contr. Conf.*, Boston, MA, Aug. 20–22, 1975.

[17] W. Hines, "Improving a simple monitor of a system with sudden parameter changes," *IEEE Trans. Inform. Theory*, vol. IT-22, July 1976.

[18] J. C. Deckert *et al.*, "F8-DFBW sensor failure identification using analytic redundancy," *IEEE Trans. Automat. Contr.*, vol. AC-22, Oct. 1977.

[19] E. G. Gai and R. E. Curry, "Failure detection by pilots during automatic landing: Models and experiments," in *Proc. 11th Ann. Conf. Manual Contr.*, Ames Research Center, Moffett Field, CA, May 1975.

[20] E. G. Gai *et al.*, "Determination of failure thresholds in hybrid navigation," *IEEE Trans. Aerospace Electron. Syst.*, vol. AES-12, Nov. 1976.

[21] D. D. Boozer and W. L. McDaniel, "On innovation sequence testing of the Kalman filter," *IEEE Trans. Automat. Contr.*, vol. AC-17, Feb. 1972.

[22] W. C. Martin and A. R. Stubberd, "An additional requirement for innovations testing in system identification," *IEEE Trans. Automat. Contr.*, vol. AC-19, Oct. 1974.

[23] M. Athans, "On the elimination of mean steady-state errors in Kalman filters," in *Proc. Symp. Nonlinear Estimation Theory*, Univ. California, San Diego, pp. 212–214, 1970.

[24] C. T. Leondes, Ed., *Control and Dynamic Systems: Advances in Theory and Applications*, vol. 12. New York: Academic, 1976.

[25] J. A. D'Appolito and K. J. Roy, "Reduced order filtering with applications in hybrid navigation," in *Proc. IEEE Electron. Aerospace Syst. Conf.*, Sept. 1973.

[26] J. I. Galdos and D. E. Gustafson, "Information and distortion in reduced-order filter design," *IEEE Trans. Inform. Theory*, vol. IT-23, Mar. 1977.

[27] F. C. Schweppe, *Uncertain Dynamic Systems*. Englewood Cliffs, NJ: Prentice-Hall, 1973.

[28] P. D. Hartman, "On the theory of confidence set estimation and detection," Ph.D. dissertation, Polytechnic Inst. Brooklyn, 1972.

[29] A. Gelb, Ed., *Applied Optimal Estimation*. Cambridge, MA: M.I.T. Press, 1974.
[30] A. H. Jazwinski, *Stochastic Processes and Filtering Theory*. New York: Academic, 1970.
[31] H. Kwakernaak and R. Sivan, *Linear Optimal Control Systems*. New York: Wiley-Interscience, 1972.
[32] J. M. Holtzman, *Nonlinear System Theory: A Functional Analysis Approach*. Englewood Cliffs, NJ: Prentice-Hall, 1970.
[33] M. Athans and F. C. Schweppe, *Gradient Matrices and Matrix Calculations*. Lexington, MA: Lincoln Lab., Nov. 1965.
[34] W. Rudin, *Real and Complex Analysis*. New York: McGraw-Hill, 1966.
[35] R. R. Goldberg, *Methods of Real Analysis*. Waltham, MA: Blaisdell, 1964.
[36] H. L. Hart, *Calculus*, Boston, MA: Heath, 1955.
[37] E. K. Blum, *Numerical Analysis and Computation Theory and Practice*. Reading, MA: Addison-Wesley, 1972.
[38] M. Abramowitz and I. A. Stegun, Eds., *Handbook of Mathematical Functions* National Bureau of Standards, (*Applied Math. Series* 55). Washington, DC: Nat. Bureau Standards, 1964.
[39] A. Papoulis, *Probability Random Variables and Stochastic Processes*. New York: McGraw-Hill, 1965.
[40] D. B. Owen, *Handbook of Statistical Tables*. Reading, MA: Addison-Wesley, 1962.
[41] A. R. DiDonato and M. P. Jarnigan, "Integration of the general bivariate Gaussian distribution over an offset ellipse," U.S. Naval Weapons Lab., Dahlgren, VA, Rep. 1710, 1960.
[42] R. J. Schulte and D. W. Dickinson, "Four methods of solving for the spherical error probable associated with a three-dimensional normal distribution," Air Force Missile Develop. Center, Holloman Air Force Base, NM, Tech. Rep. MDC-TR-68-12, Jan. 1968.
[43] T. H. Kerr, "False alarm and correct detection probabilities over a time interval for failure detection algorithms," *IEEE Trans. Inform. Theory*, to be published.
[44] M. L. Shooman, *Probabilistic Reliability: An Engineering Approach*. New York: McGraw-Hill, 1968.
[45] T. H. Kerr, "Failure detection aids for human operator decisions in a precision inertial navigation system complex," in *Proc. Symp. Applications of Decision Theory to Problems of Diagnosis and Repair* (sponsored by Amer. Statist. Ass.), Fairborn, OH, June 2–3 1976.

Decomposition Techniques for Large-Scale Systems with Nonadditive Interactions: Stability and Stabilizability

M. VIDYASAGAR, SENIOR MEMBER, IEEE

***Abstract*—In this paper, we study decomposition techniques for nonlinear large-scale systems, which have the feature that the interactions between the various subsystems are nonadditive. Using the technique of decomposing a graph into its strongly connected components, we first rewrite the system differential equations into a hierarchical form, by renumbering and aggregating the original state variables, if necessary. In this hierarchical form, each subsystem interacts only with "lower" subsystems but not with "higher" subsystems. Once the system equations have been rearranged in this hierarchical form, we show that the overall system is uniformly asymptotically stable (respectively exponentially stable, globally exponentially stable) if and only if each of the subsystems is uniformly asymtotically stable (respectively exponentially stable, globally exponentially stable). The main technique used to do this is the converse Lyapunov theory. We then turn to problems of stabilizability, and show that, once the system equations have been arranged in hierarchical form, the overall system can be stabilized by a decentralized control law if and only if each of the subsystems can be stabilized. Several examples are presented to illustrate the various theorems.**

I. Introduction

The results presented in this paper can essentially be divided into two parts. In the first part, we are interested in the stability properties of nonlinear large-scale systems described by

$$\dot{z}_i(t)=g_i(t,z_1,\cdots,z_k(t)),\qquad i=1,\cdots,k \tag{1.1}$$

where $z_i(t)$ is the state of the ith subsystem and k is the number of subsystems. Using the graph-theoretic decomposition techniques proposed in [1]–[3], it is fairly straightforward to show that the system equations (1.1) can be rearranged in the hierarchical form

$$x_i(t)=f_i(t,x_1(t),\cdots,x_i(t)),\qquad i=1,\cdots,m \tag{1.2}$$

where the new state vectors $x_1,\cdots,x_m$ are obtained from $z_1,\cdots,z_k$ by renumbering and aggregating the latter, if necessary. In [4], Michel, Miller, and Tang study the case where each function f_i is of the form

$$f_i(t,x_1,\cdots,x_i)=\sum_{j=1}^{i} f_{ij}(t,x_j) \tag{1.3}$$

and derive sufficient conditions for the stability of the overall system (1.2) involving only some properties of the "isolated subsystems"

$$\dot{x}_i(t)=f_{ii}(t,x_i(t)) \tag{1.4}$$

and the interconnection functions f_{ij} $(\cdot,\cdot),j<i$. The results in [4] can be thought of as the Lyapunov counterparts to the input–output decomposition techniques proposed in [5], [6]. Subsequently, Tang, Michel, and Hale [7], [8] extended the results of [4] to the case where the function f_i is expressible in the form

$$f_i(t,x_1,\cdots,x_i)=f_{ai}(t,x_1,\cdots,x_{i-1})+f_{ii}(t,x_i). \tag{1.5}$$

Once again, sufficient conditions for the stability of the overall system (1.2) are given in terms of the stability properties of the isolated subsystems (1.4) and the functions f_{ai}.

In the present paper, the focus is on systems of the form (1.1) with *nonadditive* interactions, i.e., where the function f_i *may not* be expressible in the form (1.5). We then introduce the "isolated subsystems"

$$x_i(t)=f_i(t,\mathbf{0},\cdots,\mathbf{0},x_i(t)) \tag{1.6}$$

and show how the decomposition techniques in [4], [7], [8] are related to the above. Finally, in the main results of this part of the paper, we show that the overall system (1.2) is uniformly asymptotically stable (respectively exponentially stable, globally exponentially stable) *if and only if* each of the isolated subsystems (1.6) is uniformly asymptotically stable (respectively exponentially stable, globally exponentially stable). We also present some conditions for the global asymptotic stability and the instability of the overall system (1.2), but these conditions are not as elegant as the others. The main tool used to accomplish all this is the converse Lyapunov theory.

In the next part of the paper, we study control systems described by

$$\dot{z}_i(t)=g_i(t,z_1(t),\cdots,z_k(t),r_1(t),\cdots,r_l(t)),\qquad i=1,\cdots,k \tag{1.7}$$

where $z_1(t),\cdots,z_k(t)$ are the state vectors and $r_1(t),\cdots,r_l(t)$ are the control functions. We show that, by renumbering and aggregating the state vectors as well as the control vectors, the system (1.7) can be rewritten in the hierarchical form

$$\dot{x}_i(t)=f_i(t,x_1(t),\cdots,x_i(t),u_1(t),\cdots,u_i(t)),\qquad i=1,\cdots,m. \tag{1.8}$$

We show that the system (1.8) can be stabilized by a decentralized control law if and only if the isolated subsystem

$$\dot{x}_i(t)=f_i(t,0,\cdots,0,x_i(t),0,\cdots,u_i(t)) \tag{1.9}$$

can be stabilized.

This paper is organized as follows. In Section II, we present the graph-theoretic technique for decomposition into hierarchical form. In Section III, we present all of the main theorems of the paper. A brief discussion of these theorems is contained in Section IV. Appendix I presents several preliminary results and definitions that are needed for the proofs of the main theorems, which are contained in Appendix II.

Manuscript received March 28, 1979; revised November 8, 1979 and January 15, 1980. Paper recommended by D. D. Šiljak, Past Chairman of the Large Scale Systems, Differential Games Committee. This work was supported by the Natural Sciences and Engineering Research Council of Canada under Grant A-7790 and the U.S. Department of Energy under Contract ET-78-C-3389.

The author was with the Department of Electrical Engineering, Concordia University, Montreal, P.Q., Canada. He is now with the Department of Electrical Engineering, University of Waterloo, Waterloo, Ont., Canada.

0018-9286/80/0800-0773$00.75